Observations and analyses of roof guttering in a coal mine

by X. Ndlovu* and T.R. Stacey*

Transaction Paper

Synopsis

Underground observations in a coal mine have indicated failure of the immediate roof above the bords. Careful observations and photographic recording of occurrences of these roof failures, termed 'roof guttering', have been made. The occurrence of guttering results directly in roof instability, and indirectly, due to the interaction of the guttering with natural planes of weaknesses in the immediate roof rock.

In this paper, relevant observations of roof guttering, possible mechanisms of formation of roof gutters, laboratory testing for determination of material strength and deformation properties, and numerical analyses to explain underground observations are described. Mapping of roof failures showed that these took place mainly towards the centre of the roadways. Roof guttering was observed often to occur violently and with little warning. Occurrence of roof guttering has a negative impact on production—some panels are abandoned, production times are increased and safety of workers is compromised. The numerical stress analyses showed that, although none of the constitutive behaviour criteria used predicted the observed underground failures correctly, the extension strain criterion gave the best agreement.

Once the root cause of roof guttering is understood it may then be possible to contain failure by optimization of excavation shape and positioning, or through the design and installation of an effective and efficient support system. The consequence would be improved safety, which should result in maximum extraction of the mineral reserves in a safe manner. The material in this paper contributes towards the understanding of stress distributions around bord and pillar geometries, the associated stress induced instability observed in a coal mine, and a better understanding of the guttering phenomenon.

Introduction

Mining of coal contributes significantly to the economy of South Africa. A significant amount of coal is exported while the main domestic uses of coal are for electricity generation, for production of oil fuels and petrochemicals, in the metallurgical industry and the cement industry (Chamber of Mines of South Africa, 2005). Coal production is mainly by bord and pillar mining, which accounts for about half of the total production and 90 per cent of the total underground production. A problem associated with bord and pillar mining of coal is roof instability. One such cause of roof instability is roof guttering, in which the roof rock fractures, falls down and leaves a groove along a roadway.

The occurrence of guttering results directly in roof instability. In addition, the guttering may interact with natural weakness planes in the roof rock, resulting in more extensive instability. Roof guttering has proved to be a safety and production constraint. It exposes miners to the hazard of rock falls, and these falls may cause damage to machinery and mine workings. In some instances endangered workings are abandoned, leading to loss of valuable mineral reserves. An important factor, which cannot be quantified, is the psychological effect on workforce of potentially unstable roof conditions (Nicholls, 1978). Rock falls are the single largest contributor to safety related fatalities in the South African mining industry (MHSC 2004/2005 Annual Report). Rock falls have accounted for about half of the accidents that cause injuries and fatalities to personnel in the coal mining industry (Van der Merwe, 1998). Figure 1 shows fatality rates for different mining sectors during the period 1994 to 2004.

Frith *et al.* (2002) noted that in most situations guttering is a result of high horizontal stresses. Van der Merwe and Madden (2002) acknowledged that the occurrence of guttering in South African coal mines is stress related. However, Van der Merwe and Peng (2000) had earlier argued that the role of horizontal stress is being exaggerated in roof instability in South African coal mines. As such, overemphasis of horizontal stress effects could result in ineffective remedial action being taken on the mines.

* *School of Mining Engineering, University of the Witwatersrand.*

 SA ISSN 0038–223X/3.00 + 0.00. Paper received Mar. 2007; revised paper received Jun. 2007.

Observations and analyses of roof guttering in a coal mine

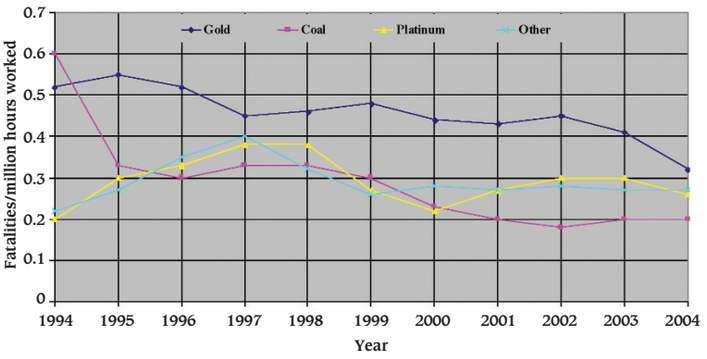

Figure 1—Fatality rates per million hours worked for South African mines 1994 to 2004 (MHSC 2004/2005 Annual Report)

To eliminate, control, or minimize the risk of rockfalls, pillar failure, and roof and floor failure as a result of the instability associated with bord and pillar mining, it is necessary to understand the distribution of stress and strain around bord and pillar geometries. It is also necessary to understand the failure mechanisms associated with roof guttering. It may then be possible to contain failure by optimization of excavation shape and positioning, or through the design and installation of an effective and efficient support system. The consequence would be safety improvement, and should result in maximum extraction of the mineral reserves in a safe manner.

Observations of roof guttering

The mapping carried out in a coal mine showed that surface features observed along a guttering roof included the upturned boat-shaped nature of a gutter, interlocking fracture surfaces towards the centre of a gutter, thin fractured slabs from the centre of gutter going outwards and a heavily fractured surface ahead of a gutter (Ndlovu and Stacey, 2005). Figure 2 illustrates the upturned boat-shaped nature of a gutter, the fractured surface and the tip of a gutter.

Figure 3 illustrates the fractured surface ahead of a gutter. On scaling down the fractured surface ahead of the gutter, roof falls occurred, which led to the gutter developing further longitudinally, laterally, and in depth. After a few hours or days another fracture surface may develop ahead of the gutter. The process repeats itself until the gutter stabilizes.

The size of gutters ranged from about 2 m in length, 0.5 m in width, and 0.1 m in depth to about 70 m in length, 3.5 m in width and 0.5 m in depth. Guttering was observed to occur most commonly towards the centre of the roadways (80%). Figure 4 shows the occurrence of guttering as mapped in one of the sections of the mine. Guttering was observed to occur predominantly in two perpendicular directions. These corresponded approximately with the horizontal principal stress directions (note that the two principal stresses are similar in magnitude).

In some areas, initiation of guttering took place within seconds of blasting while in others it occurred a few days after mining of the particular area. It was also observed that the extent of guttering progressed with time. In most instances it took several roof falls over several days for the gutter to stabilize. Guttering progression was most evident from the mining faces to about three splits back. Stresses could possibly have re-equilibrated in the back area after the guttering process, as evidenced by lack of active guttering in this area.

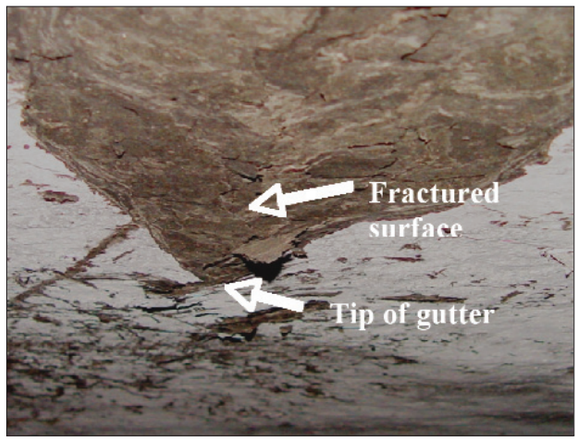

Figure 2—Upturned boat-shaped nature of guttering occurrence

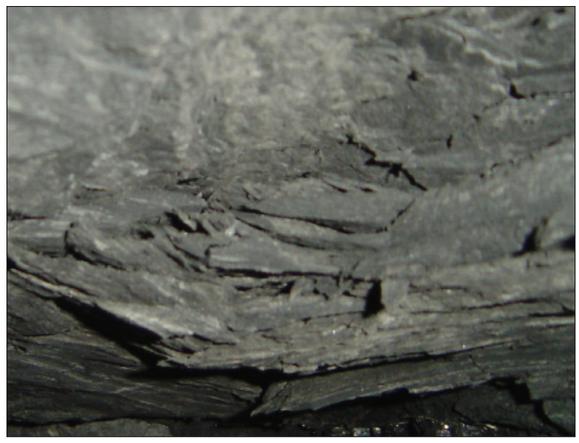

Figure 3—Stress induced fracturing ahead of a gutter; the roof gutter occurred towards the centre of a roadway

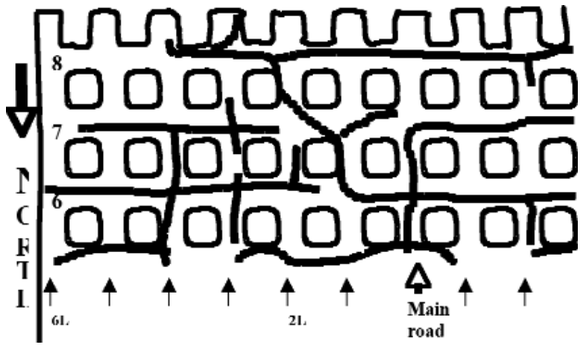

Figure 4—Occurrence of guttering in part of a section. Dotted lines represent the gutters. The numbers 6, 7, and 8 denote split number while 2L, 6L, etc. denote roadways

Possible mechanisms involved in the formation of roof gutters

The occurrence of guttering is clearly associated with high stress levels. *In situ* stress measurements carried out in the area (Munsamy, 2003; Walker and Altounyan, 2001) show that the major horizontal stress is substantially higher than the vertical stress. From the available results, horizontal to vertical stress ratios of 5.7 and 4.2 were interpreted.

To study the possible mechanisms involved in the formation of roof gutters, fracture surfaces were observed with the aid of a microscope. Thin slabs obtained from different areas in the guttering roof were used. One hundred photo images were captured during this analysis. Two of these photographs are illustrated in this paper. Figure 5 shows a fracture surface, which is believed to be of the extension type. There are no visible shear effects. Extensional type fractures were observed in about 90% of the samples. Shear type fractures were observed in a few samples (about 10%), mainly at the edges of the slabs. It is possible that the observed shear effects were due to secondary shear failure involved in the falling of rock fragments during the process of guttering. Figure 6 shows a fracture surface which is believed to be of the shear type. There are visible white surfaces caused by relative movement during the shearing process.

From underground observations it was evident that guttering involved progressive failure of brittle rock. Progressive brittle failure of rock has been extensively studied and reported by Martin (1990, 1997), Martin *et al.* (1997, 1998), Hajiabdolmajid *et al.* (2000, 2002a, 2002b, 2003), Martino and Chandler (2004), Read (2004) and Chandler (2004). The progressive failure of brittle rock discussed by the above-mentioned authors is similar to the observations of the failure of rock during the process of guttering in the coal mine. Similarities are derived from the following observations:

- Guttering involved failure of intact rock, which may be explained by stresses in the region of failure being greater than the strength of the rock in this region
- The high horizontal compressive stresses in combination with a weak mudstone roof and low compressive stresses in a vertical direction could be the main cause of the observed extension type of fractures. These fractures are parallel to the major principal stress, which is almost horizontal, and normal to the minor (sub-vertical) principal stress. Extension fractures could be initiating the process of roof guttering
- Guttering cannot be a result of high stresses alone; if this were the case, it is expected that guttering would initiate in the corners of the roadways, where induced stresses are greatest
- Occurrence of guttering was not a once-off event. Several falls of crushed rock were necessary for the gutter to stabilize. The stabilizing effect is not known. It might be possible that guttering stabilized when a more competent sandstone roof was encountered, or when stress equilibrium was reestablished after a certain advance of the roadways as demonstrated by lack of active guttering in back areas. Subsequent excavation caused stress redistribution and influenced the growth of damage and formation of new gutters. It is also possible that the same mechanism of confinement described by Martin (1997) caused the stabilization of gutter progression
- It is possible that guttering initiated in the region of maximum compressive stress concentration and propagated away from it. This is because no clear

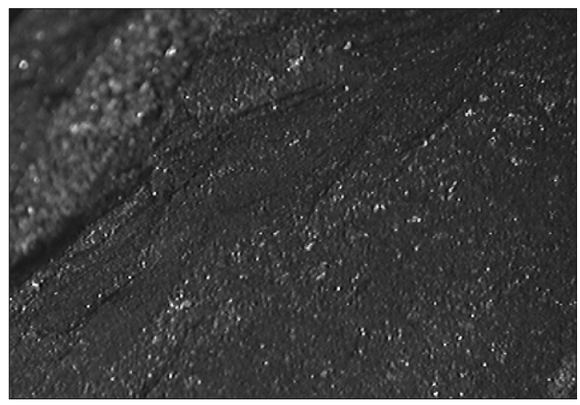

Figure 5—An extension fracture surface

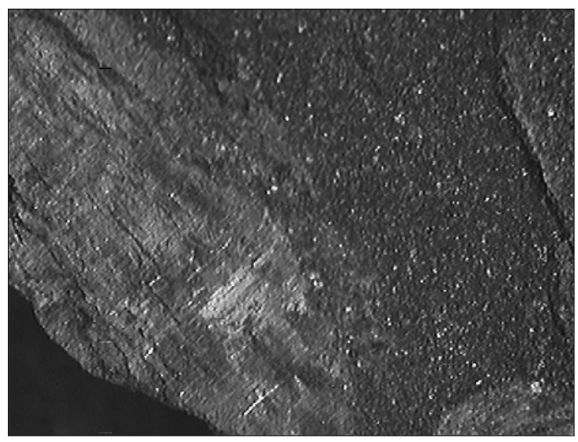

Figure 6—A shear fracture surface

pattern of the geometrical location of the occurrence of guttering was observed. In some areas, within a roadway, guttering was observed to occur on one side of the roadway, then suddenly crossed the centre of the roadway and moved to the other side of the roadway

- Scaling down favoured the progression of gutter formation. Removal of loose material, such as material previously held in place by the steel mesh support, usually helped guttering to develop further in depth, width and length.

Figures 7a and 7b show the possible geometry prior to a fall of rock during the guttering process, and the subsequent fall, respectively.

Figure 7a represents the formation of fractures a few metres from the coalface where guttering has been observed to occur. This formation, without the bulging surface, probably also occurred on occasion at the roof-coalface intersection, since guttering in some instances occurred from the coalface and propagated backwards a few minutes after blasting. An explanation could be that the roof fractures at the coalface and guttering follows immediately. This formation, without the bulging surface, probably also occurred on occasion ahead of the coalface since in some instances guttering occurred immediately on blasting. This may be explained by the assumption that the roof area ahead of the coalface already contained stress-induced fractures or that blasting removed confinement.

Occurrence of guttering grew in length, width and depth as the extension fractures continued to propagate, until a stable V-notch was reached. Slabbing was observed to play an important role in the growth of the V-notch. The process of formation and progression of gutters was observed to be mostly active from the coalface to about three splits back. This could be an area of active stress redistribution as a result of continuing mining activities.

At micro- and macro-scale it may be observed that the stages of guttering involve the following:

- *Crack initiation*—cracks could initiate behind, at, and probably ahead of the coalface in the region defined by compressive stresses exceeding the crack initiation stress
- *Process zone* (Martin, 1997)—Critically oriented flaws are exploited in the zone where the roof is very weak. Crushing occurs in a process zone about 30–60 cm wide forming extension fractures. Extensive dilation, at the grain size scale, occurs in this process zone
- *Crushing of the process zone to form gutters* (*V-notch*)—development of the process zone causes strain energy to be stored in the rock during its deformation. A point is reached where the rock cannot store any additional strain energy. The rock fails in a violent crushing manner, similar to failure in laboratory UCS tests, in the process of releasing the stored strain energy. A gutter is formed in the process
- *Slabbing*—the gutter formed exposes the bedding planes to air and moisture. The bonds between the bedding planes are weakened as a result, and slabbing takes place
- *Progression of gutter formation*—gutter formation progresses with time as extension fractures continue to propagate. It may be possible that as long as the redistributed stresses in a particular area are greater than the crack initiation stress then guttering will continue in that area
- *Stabilization*—development of a gutter stops when the stresses have apparently redistributed and a new state of stress equilibrium is established in which the growth of extension fractures is inhibited.

Laboratory testing

Laboratory testing of the shale roof rock was carried out for the purposes of obtaining the material strength and deformation properties. The purpose of determining these parameters was to provide data to be used in numerical modelling, with the object of attempting to explain the guttering process. The tests that were conducted included the following:

- Ultrasonic tests on both cylindrical and cubic samples with loading perpendicular and parallel to bedding
- Uniaxial compression tests on both cylindrical and cubic samples with loading perpendicular and parallel to bedding
- Brazilian tensile tests on cylindrical cores with loading perpendicular and parallel to bedding.

Ultrasonic tests (Brown, 1981a) were conducted to determine indicative rock anisotropy and dynamic Young's modulus. The results of the tests showed that the dynamic

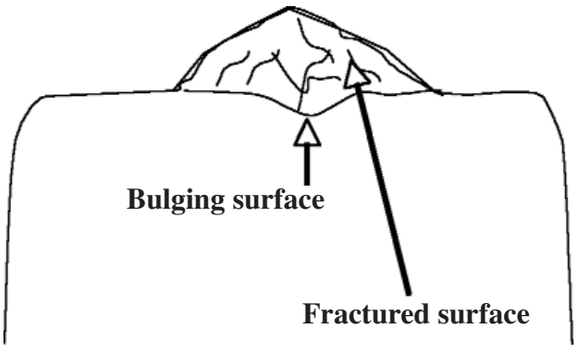

Figure 7a—Schematic diagram of a roadway cross-section showing possible fracturing just before occurrence of guttering

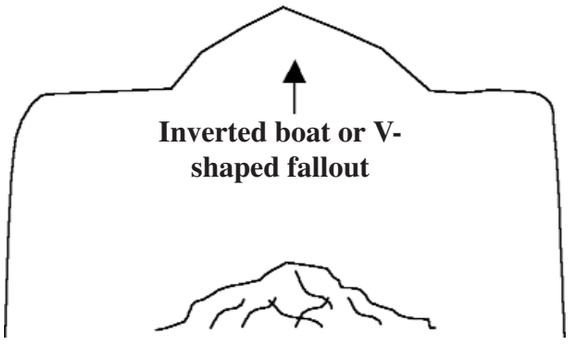

Figure 7b—Schematic diagram of a roadway cross-section showing the fallen rock and the V-shaped nature of guttered roof

Young's modulus determined parallel to the bedding was twice that determined normal to the bedding. This indicates that the rock is anisotropic.

The strain-gauged uniaxial compression test (Brown, 1981b) is used to measure the uniaxial compressive strength (UCS) of intact rock samples in the form of specimens of uniform geometry. Also derived from this test are the static deformation properties of the rock. The test results are important for strength classification, rock characterization, and as input parameters in numerical modelling software. Test results showed that UCS of intact rock is much lower for rock tested in a direction parallel to the bedding (Figure 8d) than it is for rock tested in a direction normal to the bedding (Figure 8c). This is expected as the bedding provides planes of weakness, which lower the strength of the rock.

The Brazilian tensile strength test measures, indirectly, the tensile strength of intact rock (Brown, 1981c). The results of the tests showed that samples prepared and loaded normal to the bedding (Figure 8b) have a higher tensile strength than those prepared and loaded parallel to the bedding (Figure 8a). The results of the different tests are summarized in Table I below.

From the laboratory testing programme, the mean values obtained for the numerical modelling described below were 11.3 GPa for Young's modulus, 0.27 for Poisson's ratio, 25 MPa for UCS and 1.07 MPa for tensile strength. Other input parameters, for example, friction angle, dilation angle and cohesion, were estimated.

Numerical analyses

Numerical stress analyses were carried out using a FLAC 3D model. The actual in-mine dimensions for bords and square pillars are 6.5 m and 8.7 m, respectively. For the purposes of numerical modelling bord and pillar widths assumed were 7 m and 9 m, respectively, and the modelled pillar height was 2 m. The modelled depth was 52 m below ground surface. A system of coordinate axes was defined with the origin at the horizontal plane through the pillar at pillar mid-height; the z-axis points upward and the y-axis points along the direction of mining. The two model geometries considered for the analyses are described below:

- *Model 1*—a quarter of the bord and pillar geometry was used for modelling, taking advantage of the symmetry of the excavation geometry and the loading. There are four planes of symmetry. These are the four vertical planes defining the quarter of the model. Horizontal displacements at the vertical symmetry planes are zero. To optimize memory usage and runtime requirements, only 16 m of cover was modelled, and the horizontal

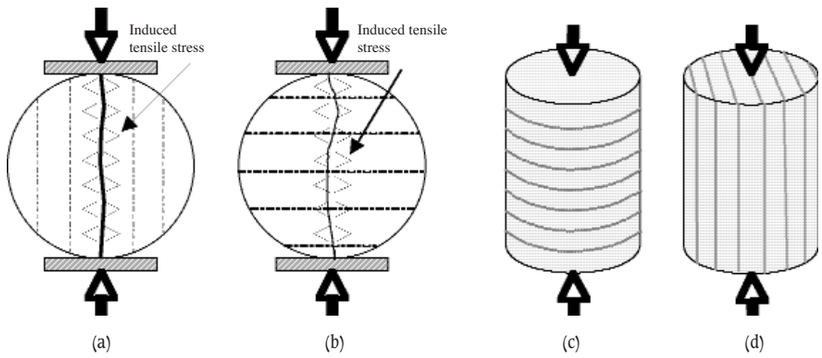

Figure 8a and b: loading along the bedding and perpendicular to the bedding, respectively, in Brazilian test; c and d: loading perpendicular to the bedding and along the bedding, respectively, in UCS tests

Table I

Results of laboratory tests

		Cylindrical specimen		Cubic specimen	
	Parallel	Perpendicular	Parallel	Perpendicular	
Density, ρ (kg/m^3)		2350			
Dynamic E (GPa)	range	16.7–19.8	10.6–11.4	19.0–20.7	9.3–9.8
	mean	18.4	11	20	9.5
Static E (GPa)	range	9.17–13.59	1.6–2.0	-	-
	mean	11.3	1.8	-	-
Static v	range	0.17–0.43	0.10–0.18	-	-
	mean	0.27	0.16	-	-
UCS(MPa)	range	23.28–28.15	37.18–40.95	23.81–28.01	36.89–39.25
	mean	25.31	39.15	25	37.8
Tensile strength (MPa)	range	0.76–1.42	2.35–3.11	-	-
	mean	1.07	2.81	-	-

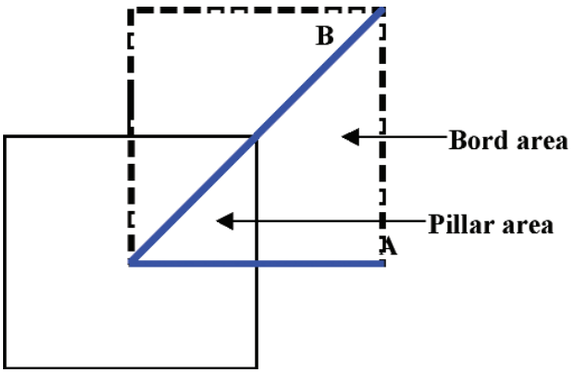

Figure 9—Plan view showing the bord and pillar quarter geometry and Lines A and B across the pillar, along which history points are located. For contour plots A becomes Section A

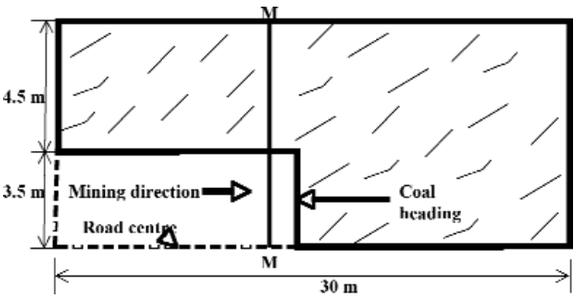

Figure 10—Plan view of model geometry with a coal heading (Line M-M/Section M-M can be moved to different locations behind and ahead of the coalface)

plane through the pillar at pillar mid-height was assumed to be another plane of symmetry. This plane was fixed in the vertical direction and the vertical displacements on it are zero. The distance of 16 m was found to be free from the influence of roadways. The quarter symmetry model is shown (dotted lines) in plan view in Figure 9. The model had 230 400 zones. The immediate shale roof is made up of zones with 0.1 m dimensions.

- *Model 2*—the geometry shows a coal heading. Loading is symmetrical. The model is shown in plan view in Figure 10. As with Model 1, four planes of symmetry were used in this model. The model contained 475 200 zones. The immediate shale roof is made up of zones with 0.1 m dimensions.

Three model analyses were carried out for each of several different material behaviours. These model analyses were:

- Model 1 described above
- Model 2 described above
- Model 1 with an interface at the coal-shale contact.

The first two assume a strong contact between the coal and shale layers. The third used an interface to allow for bed slip between the coal and the shale roof, which should have a major influence on the overall system behaviour. Selected relevant results are discussed in the following sections.

In the initiation of the analyses, an equilibrium '*in situ*' state is established before an excavation is created. The principal stress tensors show that the major principal stress is compressive throughout the model with a maximum value of 6.2 MPa. No tensile stresses exist in the equilibrium state. The major principal stress is in a horizontal direction, while the minor principal stress is in a vertical direction. The vertical stress is 1.3 MPa. Stress redistribution takes place when an excavation is created. The rock above the excavation is then supported by the pillars.

Results of elastic analyses

The isotropic and transversely isotropic models without an interface at the coal-shale contact make up the elastic models. The results for the two model analyses are discussed below.

Results of isotropic analyses

Figure 11 shows a contour plot of the vertical stress distribution after an excavation is created. High stresses exist in the pillar while the immediate roof experiences destressing. The sides of the pillar at pillar mid-height position also experiences destressing. Significant stress concentrations occur at the roof-pillar contact.

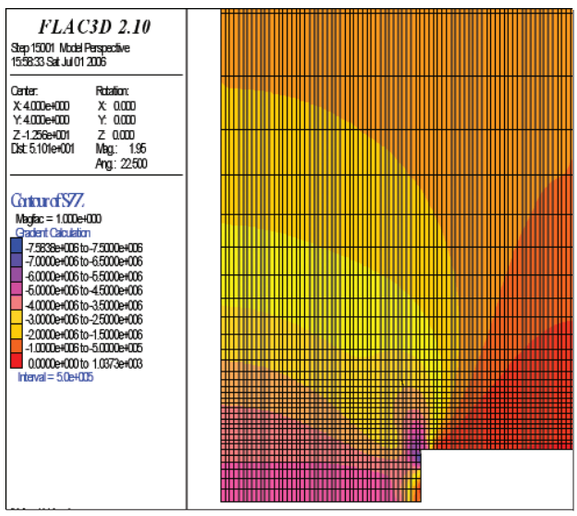

Figure 11—Contour plot of vertical stress distribution for the isotropic model (along Section A, Figure 9)

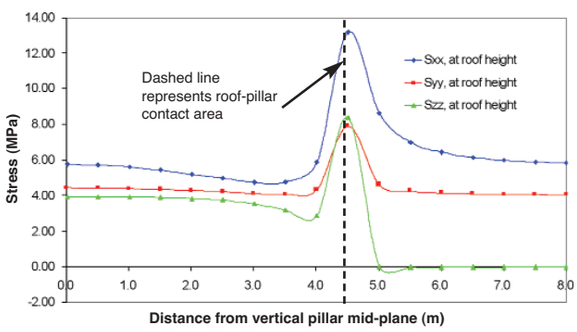

Figure 12—Distribution of stresses (along Line A, Figure 9)

Analyses of contour plots of the horizontal stress distributions show that significant horizontal stress concentrations occur at the roof-pillar contact while there is destressing around the sides of the pillar. The major and minor horizontal stresses above the roof have not significantly changed from their *in situ* values.

Figure 12 shows plots of stress distribution at the roof height position for the isotropic model. The plots show that the area that experiences high stress concentrations is very small. This area is around the roof-pillar contact and is about 1 m in width. The maximum value of the major horizontal stress is about 13 MPa, while the maximum value of the minor horizontal stress is about 6.8 MPa.

An analysis based on Model 2 geometry confirmed the above results. The distributions of the major horizontal stress at various locations behind, at and ahead of coalface are shown in Figure 13. There are, however, minor stress concentrations just behind, at and just ahead of the coalface towards the centre of the roadway. These are, however, still well below the stress concentrations at the roof-pillar contact. An analysis of the plot of principal stress tensors after excavation showed that the maximum compression is 20.3 MPa and the maximum induced tension is about 0.2 MPa. An analysis of the plot of vertical displacement shows that the maximum displacement is 1.6 mm.

Distribution of vertical stress at the pillar horizontal mid-plane shows that the peak vertical stress occurs a little inside the free face of the pillar. Results similar to these were reported by Stacey (1972) using three-dimensional finite element analyses.

Results of transversely isotropic analyses

Stress distributions are similar to those of the isotropic model. The difference exists in the magnitude of the stresses, in particular the maximum stress concentrations. An analysis of the plot of principal stress tensors after excavation indicates that the maximum compression is 23.7 MPa and the maximum induced tension is about 0.0005 MPa. A plot of displacement shows that the maximum vertical displacement is about 2.9 mm and occurs at the centre of the intersection of two roads. The peak vertical stress acting in the pillar horizontal mid-plane occurs a little inside the free face of the pillar.

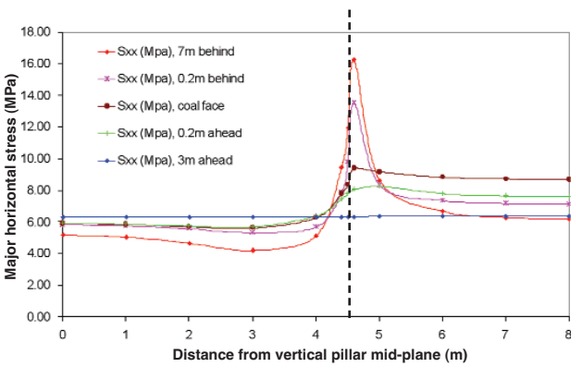

Figure 13—Distribution of major horizontal stresses (along lines parallel to M-M in Figure 10) at various positions behind, at and ahead of coalface

Results of non-elastic analyses

Non-elastic models include the isotropic and transversely isotropic models with an interface at the coal-shale contact, the Mohr-Coulomb and the Mohr-Coulomb strain softening models. The results for the analyses of non-elastic model simulations are discussed below.

Results of isotropic analyses for model with an interface

Figure 14 shows a contour plot of the vertical stress distribution for the isotropic model with an interface at the coal-shale contact. High stresses exist in the pillar, while the immediate roof experiences destressing. Small magnitudes of tensile stresses are developed towards the centre of the road, while there are no tensile stresses developed in the pillar. There are no significant stress concentrations at the roof-pillar contact.

Horizontal stress distributions show that there are no significant stress concentrations at the roof-pillar contact area. A graphical plot of the variation of stresses at different points along Line A is shown in Figure 15. The plot shows that the highest stress concentrations occur at about 0.5 m into the pillar from the roof-pillar contact area.

Distribution of vertical stress at the pillar horizontal mid-plane along Line A shows that the peak vertical stress occurs at the free face of the pillar. Results similar to these were obtained by van Heerden (1970) in his *in situ* stress measurement programme. The minimum vertical stress occurs at about 0.5 m from the free face.

Principal stress tensors show that maximum compression is 11.8 MPa, while maximum tension is 0.0004 MPa. An analysis of the displacement plots shows that the maximum vertical displacement is about 1.6 mm.

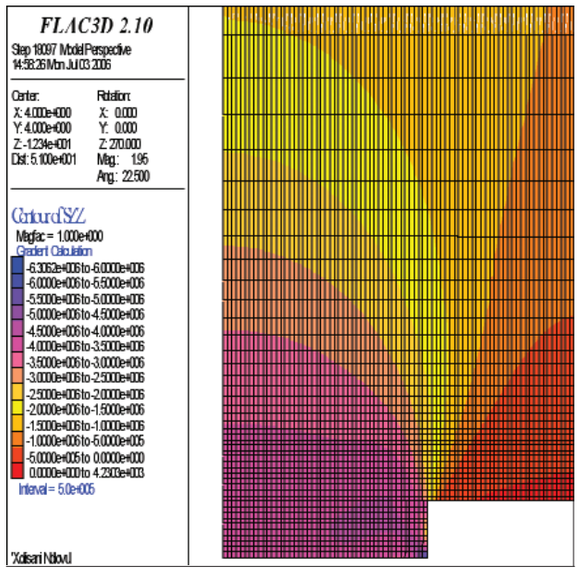

Figure 14—Contour plot of vertical stress distribution along Section A for the model with an interface

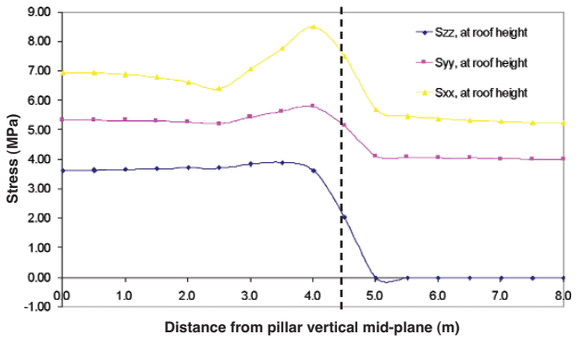

Figure 15—Distribution of stresses (along Line A, Figure 9)

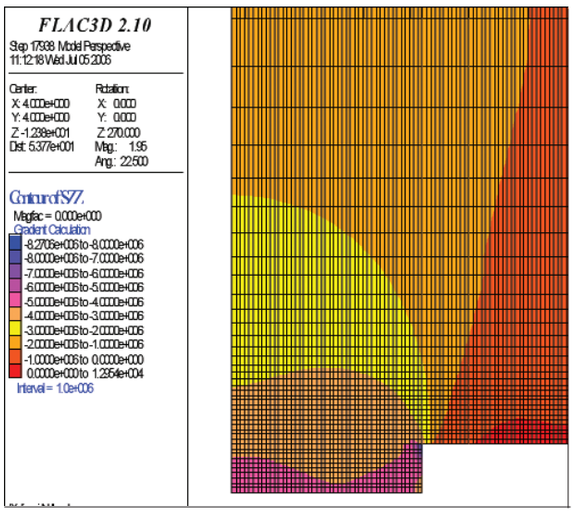

Figure 16—Vertical stress distribution (along Section A, Figure 9)

Results of transverse isotropic analyses for model with an interface

A contour plot of vertical stress distribution for this model is shown in Figure 16. The vertical stress in the pillar is compressive throughout. Tensile stresses occur towards the centre of the excavation and these are insignificant.

Analyses of major and minor horizontal stresses indicate that there are no stress concentrations towards the centre of the road. The highest stress concentrations occur mainly in the rock mass above the pillar. An analysis of the principal stress tensors show that maximum compression is 13.7 MPa, while the maximum tension very negligible at 0.0001 MPa. The displacement plots show that the maximum vertical displacement is about 3.3 mm.

Results of Mohr-Coulomb analyses

The major principal stress distribution is shown in Figure 17. The immediate roof and sides of the pillars experience significant destressing. Significant horizontal stress concentrations occur at the pillar centre. Induced tensile stresses are in the order of 0.0004 MPa in magnitude. A plot of the vertical stress distribution is shown in Figure 18. Stress concentration areas include areas along the roof-pillar contact.

Analysis of principal stress tensor plots shows that the maximum compression is about 16 MPa. Maximum tension is about 0.0004 MPa and occurs at the pillar sides. Analysis of the deformation plot indicates that the maximum vertical deformation is about 3.5 mm and occurs at the centre of the intersection.

A useful analysis tool for the Mohr-Coulomb simulations is the plot of plasticity indicators. Plasticity indicators show the zones that have failed in the past during the model run and those that are currently in a state of failure. The plot of plasticity indicators shown in Figure 19 indicates zones failing in shear in the immediate roof around the roof-pillar contact. The size of the failure region (shown by shear-n) is about 1.1 m in width and 0.5 m in height. The whole shale roof, including part of the sandstone roof, seem to have satisfied the failure criterion earlier in the model run (shown by shear-p), but now the stresses fall below the yield surface.

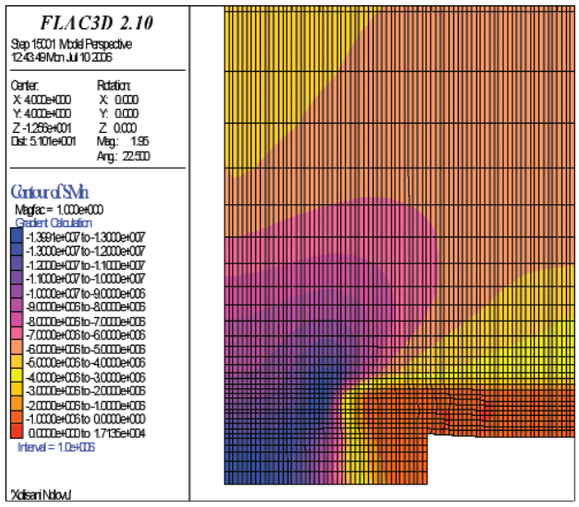

Figure 17—Plot of major principal stress distribution along Section A

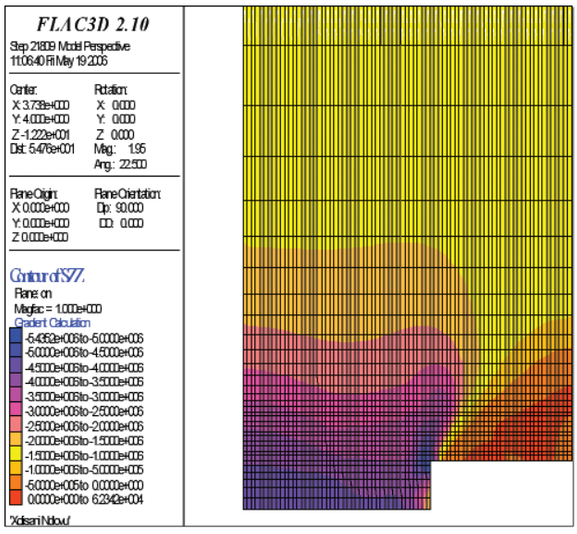

Figure 18—Plot of vertical stress distribution along Section A

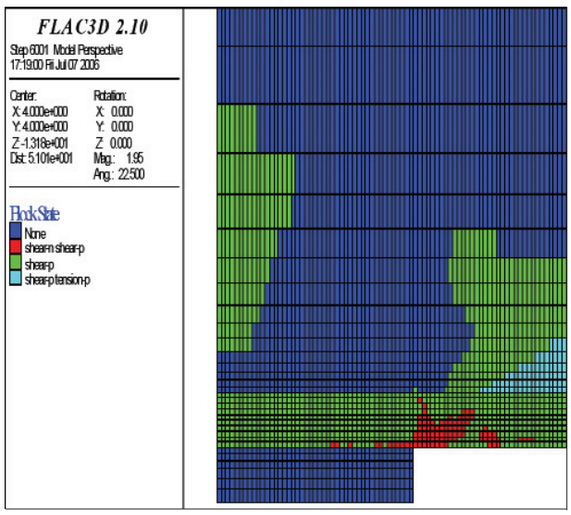

Figure 19—Failure state in the immediate roof (along Section A, Figure 9)

Initial plastic flow can occur at the beginning of a simulation, but subsequent stress redistribution unloads the yielding elements so that their stresses no longer satisfy the yield criterion.

The following analyses are for simulations based on the model with a coal heading. Figure 20 shows the failure state of the zones at the roof level. Failure occurs in the proximity of the roof-pillar contact.

Failure zones at 0.2 m behind the coalface indicate that failure is taking place for a height of about 0.4 m of the immediate roof. Failure zones at 1 m behind the coalface are shown in Figure 21. The zones are located at the roof pillar contact area and the height of failure is about 1.5 m and the width is about 0.5 m. The failure zones are inclined at about 30 degrees to the vertical. Failure at 3 m behind the coalface is similar to the failure at 1 m behind the coalface. Failure zones at 6 m behind the coalface show that failure is taking place at the roof-pillar contact. The failure is about 0.4 m in width and 1 m in height. No tensile failure took place for the model with a coal heading.

Results of Mohr-Coulomb strain softening analyses

The strain softening model analyses indicate that failure takes place towards the roof pillar contact area as shown in a section plot in Figure 22. The width of failure is about 0.5 m and the height of failure is about 0.2 m. At some time during the model run tensile strength of rock was exceeded and is indicated by 'tensile-p' in Figure 22.

The state of failure at different locations behind the coalface shows that failure initiates at the roof-pillar contact and progresses in a direction that is away from the roof and towards the area above the pillar.

The results for the model with an interface between the coal and shale contact also show failure in the proximity of the roof-pillar contact as shown in plan view in Figure 23. The region that is currently failing is about 0.5 m in width around the roof-pillar contact area.

Principal stress tensor plots show that the maximum compression is about 10.2 MPa. Maximum tension is about 0.5 MPa and occurs at the pillar sides. Analyses of the deformations show that the maximum vertical deformation is about 4.2 mm and occurs at the centre of the intersection.

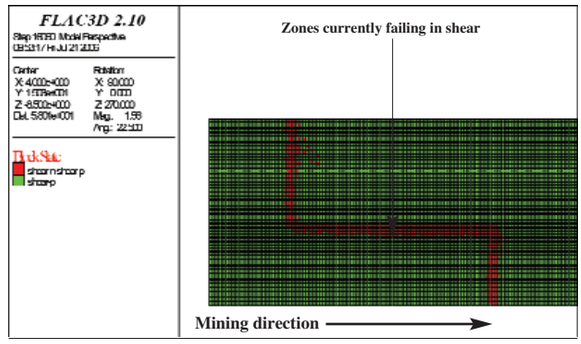

Figure 20—Plan view showing failure zones at the roof level for model with a coal heading

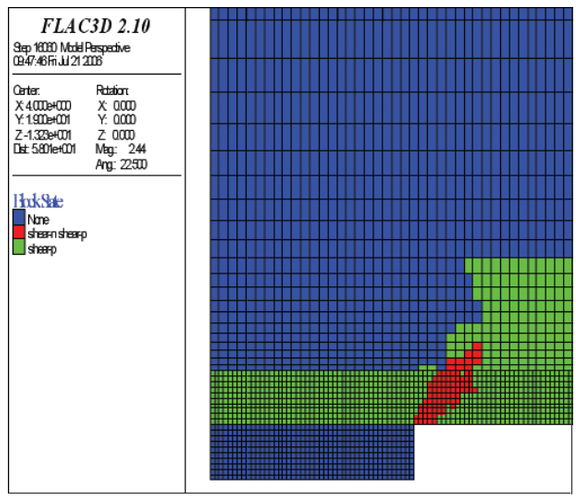

Figure 21—Failure zones 1 m behind the coalface (along line parallel to Section M-M, Figure 10)

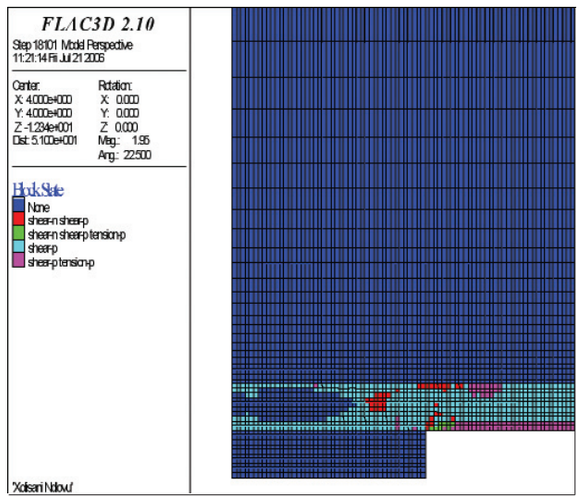

Figure 22—Failure state above immediate roof for strain softening model (along Section A, Figure 9)

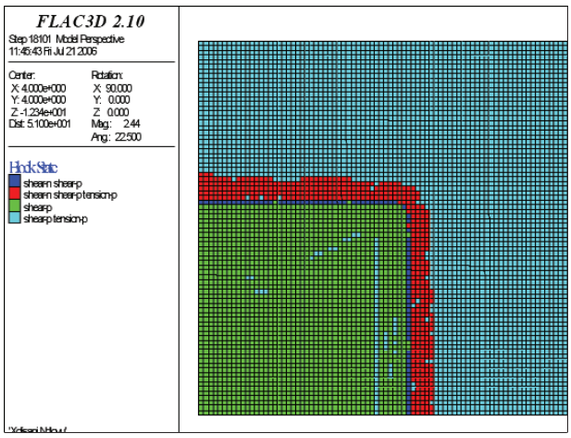

Figure 23—Plan view showing failure state at the roof level for Model 1 geometry with an interface

Results of extension strain analyses

Extension strain has been used as a criterion to predict fracture of rock (Stacey, 1981) and therefore its application to the prediction of the occurrence of guttering was considered. Extension strain analyses were based on results from some of the models described above, as summarized in the following:

- Isotropic model without an interface (based on Models 1 and 2)
- Isotropic model with an interface (based on Model 1)
- Transversely isotropic model without an interface (based on Models 1 and 2)
- Transversely isotropic model with an interface (based on Model 1).

The analyses are presented in the form of extension strain magnitudes and distributions. Extensions are negative strains, but are presented here as positive for plotting purposes. Results are presented in the form of plan views of extension strain values and distributions at the roof level. Plan views at other locations in the immediate roof are included for comparison purposes. Section plots are included where these are deemed necessary. The results showed that extension occurs pervasively in the exposed roof. Details of the strains calculated in the analyses are summarized below.

- *Isotropic model without an interface*—extension strain distribution in the immediate roof varies between 240 microstrains and to just above 320 microstrains, as shown in Figure 24. Extension strain values are highest at the roof-pillar contact area and decrease towards the centre of the road. Towards the centre of the road the extension strain value is constant at between 240 and 250 microstrains for the entire immediate shale roof.
  At other locations the extension strain values decrease with height into the roof. For example, the extension strain value of above 320 microstrains occurs for only 0.3 m of the immediate roof and just above this area extension strain values of less than 180 microstrains occur.

Figure 25 shows the extension strain distribution at the roof level, while Figure 26 shows the extension strain distribution at 1 m above the roof level. The distribution of high

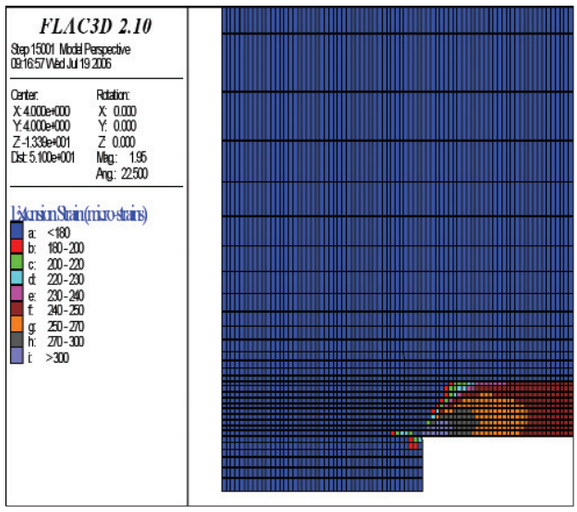

Figure 24—Extension strain distribution (along Section A, Figure 6.4)

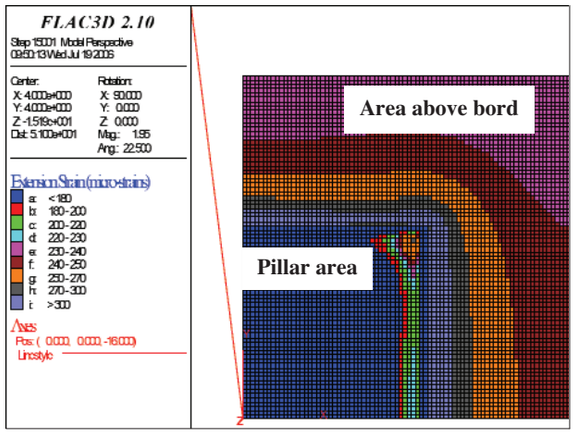

Figure 25—Plan view of extension strain distribution at roof level

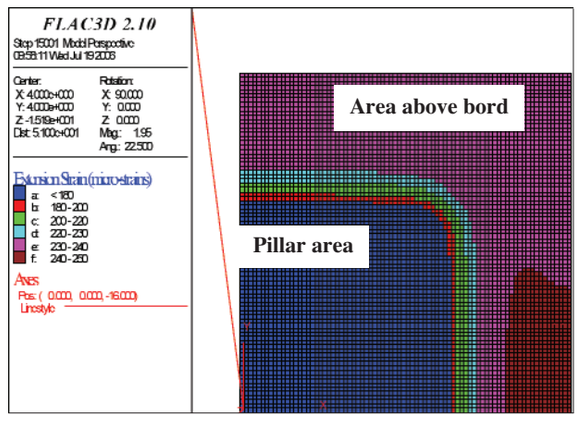

Figure 26—Plan view of extension strain distribution at 1 m above roof level

extension strain values is more prominent in the road that is orientated normal to the direction of the maximum *in situ* horizontal stress than it is in the road orientated along this direction.

The quarter model represents a situation that exists well behind the coalface where pillars have been demarcated. At such areas few instances of initiation of roof guttering were observed. Analyses based on Model 2 geometry shows similar extension strain magnitudes. The model shows that a constant extension strain magnitude of 240–250 microstrains occurs at the centre of the road for the whole immediate shale roof. The extension strain distribution at the roof level is shown in Figure 27. High extension strains also occur at the centre of the road just behind the coalface, at roof level position, possibly because this is a roof-pillar contact area. Extension strains as high as 270 microstrains also occur just ahead of the coalface at about 0.5 m from the roof-pillar contact area to the centre of the road.

At the coalface the area that experiences significant extension strain is the roof height position over a depth of only 0.1 m. At this location the extension strain varies from 180–200 microstrains. Extension strains as high as 270 microstrains occur just ahead of the coalface at about 0.5 m from the roof-pillar contact area as can be seen in Figure 27. At about 1.4 m ahead of the coalface the only significant (180–200 microstrains) occurrence of extension strain is at the centre of the road, as shown in Figure 28. It occurs some 0.4 m to 0.9 m above the roof level position and over a width of 1.2 m.

- *Isotropic model with an interface*—the extension strain values vary between 220 and 270 microstrains in the immediate shale roof, as shown in Figure 29. This is a big difference when compared to the model without an interface where extension strain values vary between 240 and 320 in the immediate shale roof. High extension strains occur towards the roof-pillar contact area. Plan views of extension strain distributions show that the area covered by each range of the extension strains is equal in the two perpendicular roads. This can be observed from Figure 30, which shows the extension strain distribution at 1 m above the roof level

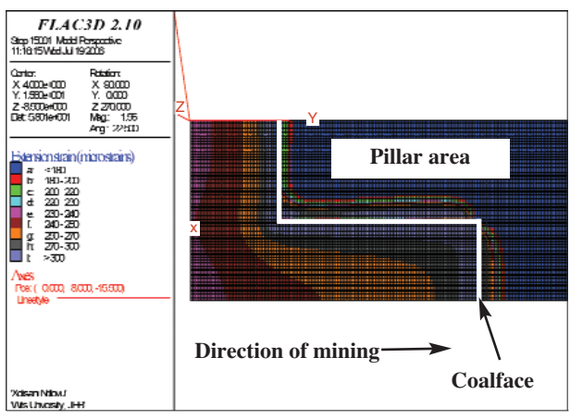

Figure 27—Plan view of extension strain distribution at roof level (based on Model 2 geometry)

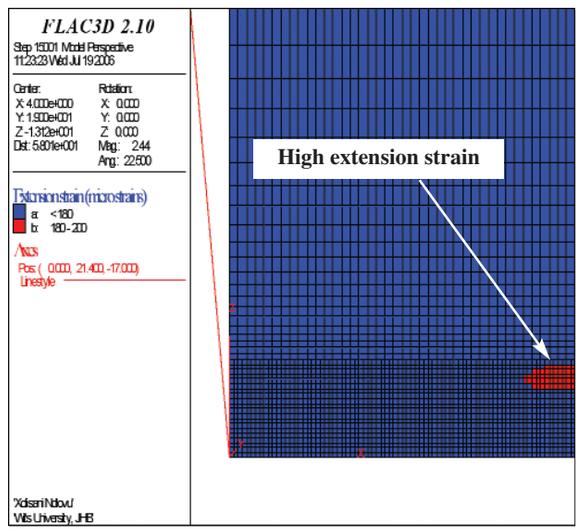

Figure 28—Extension strain distribution at 1.4 m ahead of the coalface (along section parallel to M-M, Figure 9)

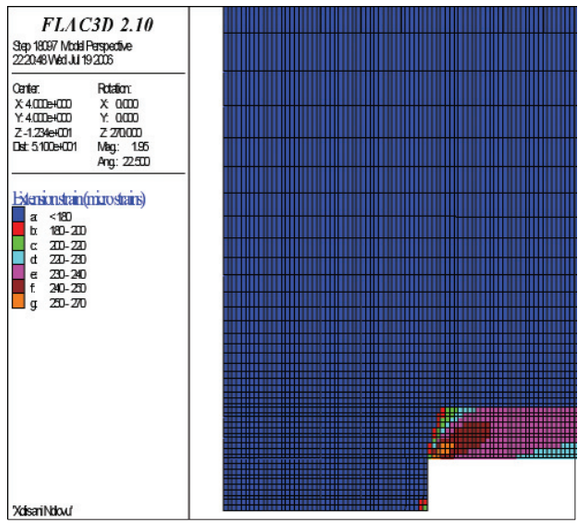

Figure 29—Extension strain distribution (along Section A, Figure 9)

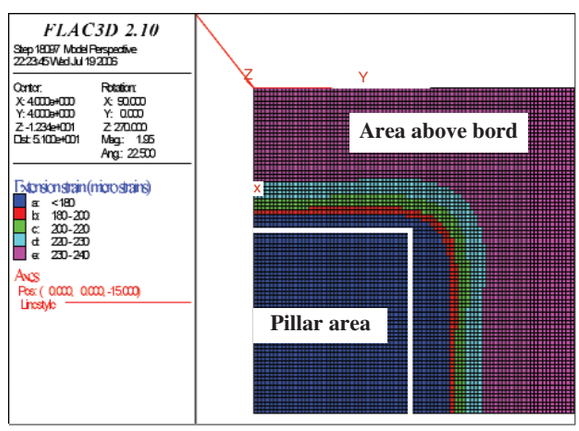

Figure 30—Plan view showing extension strain distribution at 1 m above the roof level position

position. The Figure also shows that the highest extension strains (230–240 microstrains) at this height occur towards the road centre.

- *Transversely isotropic model without an interface*—high extension strains occur above the road along the direction of mining. The road is orientated normal to the direction of the maximum *in situ* horizontal stress. The plot of extension strain distribution at roof level is shown in Figure 31. There are also high extension strain values (250–270 microstrains) just ahead of the coalface.
- *Transversely isotropic model with an interface*—extension strain values calculated based on this model are in the range of 220 to 300 microstrains in the immediate roof, as shown in Figure 32. The majority of zones have an extension strain in the region of 200–220.

Analyses of results and comparison with mine observations

A comparison of the results of the different analyses is made and presented here. The comparisons are based on the state of stress in the immediate roof, maximum compression, tension and vertical displacements, maximum induced stress along Section A, location of the highest induced stress and the state of horizontal stress at the centre of the bords in the immediate roof. Table II is a summary of the results.

The results show that higher compression is developed in the elastic (isotropic and transversely isotropic) models than in the non-elastic models. The Mohr-Coulomb model with an interface and the Mohr-Coulomb strain softening models have the lowest compression at about 10 MPa. All the models show insignificant induced tension in the immediate roof. The high horizontal stresses at the mine could be inhibiting sagging of the roof and development of tensile stresses. In all the analyses the induced displacements (strains) are insignificant despite the use of the large strain mode in

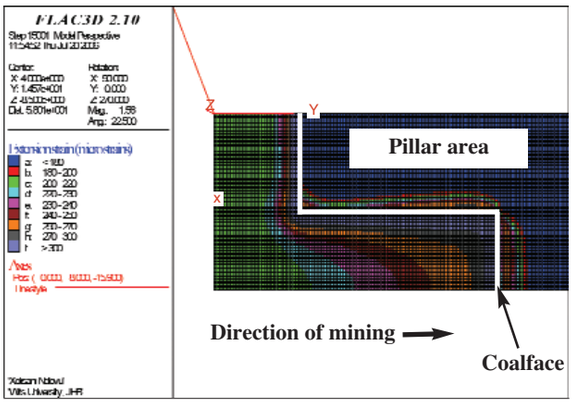

Figure 31—Plan view of extension strain distribution at roof level

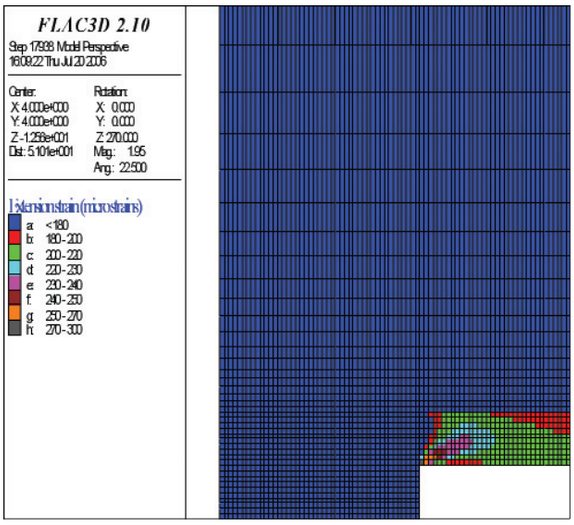

Figure 32—Distribution of extension strain (along Section A, Figure 9)

Table II

Comparison of results for the different constitutive behaviours

Constitutive law	Maximum compression (MPa) σ_1	Maximum tension (MPa) σ_2	Maximum displacement (mm) σ_3	Maximum induced stress along Section A (MPa) of the road			Location of highest induced stress	Horizontal stress state at the roof above centre
Isotropic	20.3	0.2	1.6	14.5	6.8	4.3	Roof-pillar contact area	Slight stress concentration
Transversely isotropic	23.7	0.0005	2.9	16.5	9.2	4.7	Roof-pillar contact area	Slight stress concentration
Isotropic with interface	11.8	0.0004	1.6	11.2	5.8	3.9	0.5 m into the pillar from roof-pillar contact	Insignificant destressing
Transversely isotropic with interface	13.7	0.0001	3.3	11.2	7.5	4.2	Above the roof-pillar contact area	Insignificant destressing
Mohr-Coulomb	16.0	0.0004	3.5	14.0	8.4	7.9	Roof-pillar contact area	Significant destressing
Mohr-Coulomb with interface	10.2	0.2	3.0	9.0	5.2	4.0	Above the roof-pillar contact area	Significant destressing
MC strain softening	10.0	0.5	3.8	9.7	6.0	5.9	Roof-pillar contact area	Significant destressing
MC strain softening with interface	10.2	0.5	4.2	9.3	6.0	5.4	Above the roof-pillar contact area	Significant destressing

FLAC3D analyses. Underground observations did not indicate any observable sagging of the roof (no measurements were made), nor any delamination due to the anisotropy of the rock. The results of induced displacements obtained from the 'continuous' model can, therefore, be said to represent the situation at the mine. The highest stress concentrations occurred around the roof-pillar contact area for all the models without an interface. For the models with an interface the highest stress concentrations occurred in the area above the pillar and away from the roof-pillar contact area. The interface allowed sliding at the coal-shale contact, hence the observed results.

Slight stress concentrations towards the centre of the road were predicted for the elastic models. These were well below the stress concentrations predicted at the roof-pillar contact area. Failure is expected to initiate and occur at the roof-pillar contact area. The isotropic and transversely isotropic analyses with an interface at the coal-shale contact did not show any significant stress concentrations close to the vicinity of the excavation. Stress concentrations in the two models occur inside the pillar. There is insignificant destressing in the immediate roof. It is difficult to predict where initiation of failure should take place using the two models as there are no stress concentrations in the vicinity of the excavations.

The non-elastic Mohr-Coulomb and Mohr-Coulomb strain softening analyses show that there is destressing in the immediate roof. Stress concentrations, as in the elastic analyses, occur at the roof pillar contact area. The models predict shear failure at the roof-pillar contact area. From underground observations the majority of failures initiated and occurred towards the centre of the roadways, away from the roof-pillar contact area. The Mohr-Coulomb and Mohr-Coulomb strain softening analyses, however, predicted the failures that occur towards the roof-pillar contact area. Predicted failure is up to 1 m in depth while underground observations showed that the depth of failure is up to 0.5 m. The predicted width of failure is about 1.1 m, while underground observations showed failure widths of up to 3.5 m. The models therefore overpredicted the depth of failure and underpredicted the width of failure.

The analyses showed that substantial extension strains are present in the roof. High extension strain values occurred in the proximity of the roof-pillar contact. Extension strain values are as high as 320 microstrains. Initiation of failure could be at strains in the region of 90 microstrains calculated from the formula below:

$$e_{ini} = \sigma_t / E$$

where e_{ini} = extension strain at initiation of fracture
σ_t = tensile strength of rock
E = Young's modulus

Failure of rock could be taking place at strain values that are about three times the failure initiation strain values. This translates to about 270 microstrains. Using the value of 270 microstrains as the value that signifies the onset of failure, then the predicted depth of failure is about 0.5 m and the width of failure is up to about 2 m. Failure that occurred towards the roof-pillar contact area underground is therefore well predicted by the extension strain criterion, both in depth and width. The distribution of high extension strain values is more prominent in the road that is orientated normal to the direction of the maximum *in situ* horizontal stress than it is in the road orientated along this direction.

All of the above models showed that the most likely location of failure initiation and development is at the roof-pillar contact, which demonstrates a mismatch between analysis results and observations. For this reason, the model with a coal heading was run, and this showed that the highest value of extension strain (180–200 microstrains) occurrence, at about 1.5 m ahead of the coalface, is at the road centre. This model therefore indicated that fracture initiation could be taking place at this location ahead of the coalface. It is possible that, on blasting, the rock in which fractures have initiated, fails and in the process forms a roof gutter at the centre of the road. This then corresponds with the observations of failure location at the mine in question.

It should be noted that extension strain analyses are implemented on models that have been stepped to equilibrium. The induced principal stresses used in the calculations have been shown to be elevated at the roof-pillar contact area. This could be a reason why high extension strains are predicted at the roof-pillar contact. An implementation of the extension strain criterion based on removal of zones whose extension strain exceeds a critical value also predicted failure at the roof-pillar contact area.

Conclusions from numerical analyses

Numerical modelling results have indicated that there are insignificant stress concentrations towards the centre of the roadway using the elastic and transversely isotropic elastic models. Stress concentrations were predicted at the roof-pillar contact area. It is therefore expected, from predictions using numerical analyses, that failure should initiate and occur at the roof-pillar contact area. This does not correspond with the underground observations of guttering.

The Mohr-Coulomb and Mohr-Coulomb strain softening models predicted shear failure at the roof-pillar contact area. The predicted depths of failure ranged from about 0.2 m to about 1.5 m, while the predicted widths of failure ranged from about 0.4 m to about 1.1 m. The observed underground failures ranged from about 0.1 m to 0.5 m in depth and from about 0.5 m to 3.5 m in width. The two models, therefore, overpredicted the depth and underpredicted the width of failures.

Extension strain analyses predicted failure mainly at the roof-pillar contact area. The depths and widths of failure were successfully predicted. High extension strain values were also predicted at the centre of the road position ahead of the coalface. It is possible that fracture initiation could be taking place ahead of the coalface. On blasting, the rock that has been fractured fails and, in the process, a gutter is formed at the centre of the road.

Conclusions

The occurrence of roof guttering in the roof of a local coal mine has been mapped and results presented in this paper. It has been shown that about 80% of the occurrence of roof guttering initiates and occurs towards the centre of the roads rather than in the roof-pillar contact area. The following conclusions were drawn from the thorough mapping exercise:

- Guttering occurs mainly towards the centre of the bords (80%). Only about 20% of the guttering occurs at the roof-pillar contact area. Guttering involved failure of intact rock and not failure of a rock mass containing natural weakness planes
- Special features of the formed gutters are the boat shape, fracture surfaces ahead of the gutter and towards the centre of the gutter, the explosive sound during formation of the gutters, and the progressive nature of formation of the gutters
- Observation of fracture surfaces of the rock obtained from guttering roof indicated that about 90% of the surfaces showed extension type of failure. The remaining 10% showed shear failure. The shear failure can possibly be attributed to shearing on surfaces when rock falls during the process of guttering
- Guttering does not appear to be a result of high stresses alone; if this were the case it is expected that guttering would initiate in both corners of the roadways, where the stresses are highest
- Laboratory results confirmed that the shale/mudstone roof rock was weak, with an average uniaxial compressive strength of 27 MPa, and that the rock was transversely isotropic. The tensile strength was as low as 1 MPa.

Three-dimensional stress and strain analyses of a bord and pillar geometry in a coal mining environment using the FLAC3D code have been presented in this paper. In addition, the analyses were carried out to study the phenomenon of roof guttering, which formed the greater part of the investigation. The following conclusions have been drawn from these analyses:

- The immediate roof was destressed while the pillar developed significant induced stresses, especially the vertical stresses. The greatest stress concentrations occurred at the roof-pillar contact area
- Displacements were of the order of a few millimetres. There was no observable sagging of the roof and the small displacements obtained from numerical analyses therefore agree with underground observations. The high horizontal stresses that exist at the mine could be inhibiting sagging of the roof
- Isotropic and transversely isotropic numerical analyses showed that there were slight stress concentrations towards the centre of the road, but significant stress concentrations at the roof-pillar contact area. It is therefore expected that if any failure takes place it should initiate at the roof-pillar contact
- Analyses based on the traditional Mohr-Coulomb constitutive behaviour predicted shear failure at the roof-pillar contact area. The predicted depths of failure ranged from about 0.4 m to about 1.5 m, while the predicted widths of failure ranged from about 0.4 m to about 1.1 m. The observed underground failures ranged from about 0.1 m to 0.5 m in depth and from about 0.5 m to 3.5 m in width. The model, therefore, overpredicted the depth and underpredicted the width of failures
- The Mohr-Coulomb strain softening model also predicted shear failure towards the roof-pillar contact. The predicted depth of failure was about 0.2 m, while the predicted width of failure was about 0.5. The model, therefore underpredicted both the depth and width of failure
- The analyses showed that substantial extension strains are pervasive in the roof. Implementation of the extension strain criterion showed that high extension strain values occur at the roof pillar contact for models without an interface. These models represent a situation where the coal-shale contact is strong. Few occurrences of roof-guttering were observed at the roof pillar contact.
- The extension strain criterion predicted correctly the depth and width of failures, although the failures were predicted at the roof-pillar contact area, while the observations indicated failure mainly towards the centre of the roads
- Initiation of failure was predicted ahead of the coalface at the centre of the road position using the extension strain criterion.

Although none of the constitutive behaviours predicted correctly the observed underground failures, the extension strain criterion has shown the best agreement. Guttering that occurred at the roof-pillar contact was predicted successfully using the extension strain criterion. The extension strain criterion predicted initiation of failure ahead of the coalface at the road centre position. It is possible that fracture initiation could be taking place ahead of the coalface. On blasting, the rock in which fractures have initiated fails and, in the process, a gutter is formed at the centre of the road.

Acknowledgements

The research described in this paper was carried out by the first author for an MScEng dissertation. The research was funded through a bursary provided by SIMRAC, the Safety in Mines Research Advisory Committee, and this funding is gratefully acknowledged. The assistance of Anglo Coal is appreciated.

References

Brown, E.T. (ed.). *Rock Characterisation, Testing and Monitoring, ISRM Suggested Methods*, Pergamon Press, New York, 1981a. pp. 105–110.

Brown, E.T. (ed.) *Rock Characterisation, Testing and Monitoring, ISRM Suggested Methods*, Pergamon Press, New York, 1981b. pp. 113–116.

Brown, E. T., (ed.) 1981c, *Rock Characterisation, Testing and Monitoring, ISRM Suggested Methods*, Pergamon Press, New York, pp. 119–121.

Chamber of Mines of South Africa. 2004. INTERNET. http://www.bullion.org.za. Cited 10 May 2005.

Frith, R.C., Thomas, R., Hill, D., and Buddery, P. Final Project Report—Survey of horizontal stresses in coal mines from available measurements and mapping, SIMRAC Project COL802, 2002. 51 pp.

Hajiabdolmajid, V., Kaiser, P. K., and Martin, C. D. Modelling brittle failure of rock. *Int. J. Rock Mech. and Min. Sci*. vol. 39, 2002a. pp. 731–741.

Hajiabdolmajid, V., Kaiser, P. K., and Martin, C.D. Mobilisation of strength in brittle failure of rock—in laboratory vs. *in situ*. Mining and Tunnelling Innovation and Opportunity. *Proceedings of the 5th North American Rock Mechanics Symposium and the 17th Tunnelling Association of Canada Conference*: NARMS-TAC 2002. 2002b.

HAMMAH, R., BAWDEN, W., CURREN, J., and TELESNICKI, M. (eds.), vol. 1, University of Toronto, pp. 227–234.

HAJIABDOLMAJID, V., KAISER, P. K., and MARTIN, C.D. Mobilised strength components in brittle failure of rock. *Geotechnique*, vol. 53, no. 3, 2003. pp. 327–336.

HAJIABDOLMAJID, V., MARTIN, C. D., and KAISER P. K. Modelling brittle failure of rock. *Pacific Rocks 2000*, Girand, Liebman, Breeds and Doe (eds.). Balkema, Rotterdam. 2000.

MARTIN, C.D. Characterising *in situ* domains at the AECL Underground Research Laboratory. *Can. Geotech*. J, no. 27, 1990. pp. 631–646.

MARTIN, C.D. Seventeenth Canadian Geotechnical Colloquium: The effect of cohesion loss and stress path on brittle rock strength. *Can. Geotech. J,* vol. 5, no. 34, 1997. pp. 698–725.

MARTIN, C.D., KAISER, P.K., and MCCREATH, D.R. Hoek-Brown parameters for predicting the depth of brittle failure around tunnels. *Can. Geotech. J,* no. 36, 1998. pp. 136–151.

MARTIN, C.D., READ, R.S., and MARTINO, J.B. Observation of brittle failure around a circular test tunnel. *Int. J. Rock Mech. Min. Sci. & Geomech. Abstr*. vol. 34, no. 7, 1997. pp. 1065–1073.

MARTINO, J.B. and CHANDLER, N.A. Excavation-induced damage studies at the Underground Research Laboratory. *Int. J. Rock Mech. and Min. Sci.* vol. 41, 2004. pp. 1413–1426.

MHSC 2004/2005 Annual Report, 2005. INTERNET. http://www.mhsc.org.za. Cited 10 June 2006.

MUNSAMY, L. Determination of the high horizontal stresses at Nooitgedacht Colliery and strategies to overcome the roof instability. MINN594 Investigational Project, School of Mining Engineering, University of the Witwatersrand, 2003. 76 pp.

NDLOVU, X. and STACEY, T.R. Observations of roof guttering in a coal mine. *Proc. 3rd Southern African Rock Engng Symp. 'Best Practices in rock engineering'*, Randburg, S. Afr. Inst. Min. Metall., Symposium series S41, 2005. pp. 285–300.

NDLOVU, X. Three dimensional analyses of stress and strain distributions around bord and pillar geometries. MSc. Dissertation, University of the Witwatersrand, 2006. 171pp.

NICHOLLS, B. Pillar extraction on the advance at Oakdale Colliery. Stability in Coal Mines. *Proceedings of the First International Symposium on Stability in Coal Mining*, Vancouver, British Columbia, Canada, 1978. pp. 182–196.

STACEY, T.R. Three-dimensional finite element stress analysis applied to two problems in rock mechanics. *J. S. Afr. Inst. Min. & Metall*., vol. 72, no. 10, 1972. pp. 251–256.

STACEY, T.R. A simple extension strain criterion for fracture of brittle rock, *Int. J. Rock Mech. Min. Sci*., vol. 18, 1981. pp. 469–474.

VAN DER MERWE, J.N. and PENG, S.S. Recent developments in rock engineering for coal mines—notes on the International Conference on Ground Control in Mines. *The Future, 12th International Conference on Coal Research*, The S. Afr. Inst. Min & Metall., Johannesburg. 2000.

VAN DER MERWE, J.N. *Practical Coal Mining Strata Control: A Guide for Managers and Supervisors at all Levels*. Jack Brillard Printing Services C. C., Johannesburg. 1998.

VAN DER MERWE, J.N. and MADDEN, B.J. Rock Engineering for Underground Coal Mining, *S. Afr. Inst. Min. & Metall*., Special Publications Series 7, Johannesburg. 2002.

VAN HEERDEN, W.L. Stress measurements in coal pillars. *Proc. 2nd Congr. Int. Soc. Rock. Mech*., Belgrade, vol. 2, Theme 4, Paper No. 16, 1970. 5 pp.

WALKER, G. and ALTOUNYAN, P. *In situ* stress measurements at Nooitgedacht, No. 5 Seam Section 50/51, Rock Mechanics Technology (Pty) Ltd Report to Greenside Colliery, AngloCoal, 2001. 14 p. ◆